Theor Chem Acc (2010) 126:151–163
DOI 10.1007/s00214-009-0615-z

REGULAR ARTICLE

Multicentered effective group potentials: ligand-field effects in organometallic clusters and dynamical study of chemical reactivity

Christophe Raynaud · Iker del Rosal · Franck Jolibois · Laurent Maron · Romuald Poteau

Received: 5 June 2009 / Accepted: 19 July 2009 / Published online: 8 August 2009

Abstract A new multicentered effective group potential (EGP) is obtained for η^6-benzene. Applications on $[Ru_4(H)_4(C_6H_6)_4]^{n+}$ clusters ($n = 0$ or 2) are in excellent agreement with reference DFT studies in terms of geometries, energies and electronic structures. In particular, the small singlet–triplet energy difference (3.8 kcal mol^{-1}) in $[Ru_4(H)_4(C_6H_6)_4]^{2+}$ is very well reproduced. This new EGP is nevertheless not free from the limitations associated to this first generation of molecular pseudopotentials. A cautious analysis of the nature and exact role of this EGP is made, which provides new directions for the elaboration of the next generation of EGPs. In addition, the η^5-cyclopentadienyl EGP has been used to perform a constrained dynamical simulation for the reaction of Cp_2LaH with H_2. The energy conservation during the simulation as well as the activation barrier extracted from the simulation clearly demonstrate the good behavior of this EGP in the context of molecular dynamics. Anharmonic effects on this reaction are underlined, further demonstrating the high accuracy of the potential energy surface obtained with EGPs. From a more general point of view, such EGPs are expected to provide accurate albeit low-cost ligand-field effects in organometallic clusters or nanoparticles and to allow dynamical studies at the surface of such compounds.

Keywords Effective group potentials · Ab initio molecular dynamics · Organometallic clusters and nanoparticles · Chemical reactivity

Dedicated to the memory of Professor Jean-Pierre Daudey and published as part of the Daudey Memorial Issue.

C. Raynaud
Institut Charles Gerhardt, CNRS 5253, Université Montpellier 2, CC 1501 Place Eugène Bataillon, 34095 Montpellier, France

I. del Rosal · F. Jolibois · L. Maron · R. Poteau (✉)
Université de Toulouse, INSA, UPS, LPCNO, IRSAMC, 135 avenue de Rangueil, 31077 Toulouse, France
e-mail: romuald.poteau@univ-tlse3.fr

I. del Rosal · F. Jolibois · L. Maron · R. Poteau
CNRS, UMR 5215 (IRSAMC), 31077 Toulouse, France

1 Introduction

Organometallic nanoparticles (NPs) elicit a great interest due to their physical and chemical properties intermediate between small molecular compounds and the bulk material, resulting from surface or quantum size effects [1]. Quantum chemists face a challenge, owing to the size of these species and the difficulty to determine their wavefunction. Three complementary approaches may bring different insights: (a) the bottom-up route, which consists in the accurate description of small organometallic clusters and in an extrapolation to NPs, (b) the top-down route, which consists in the description of ligands adsorbed at the surface of slab models by means of periodic quantum chemistry methods, (c) the actual description of NPs, which may be achieved by density functional theory (DFT) methods, but which are rather the scope of semi-empirical approaches [2]. Recently, structural and spectroscopic properties of scale models of ruthenium NPs have been investigated: several $[Ru_4]$ and $[Ru_6]$ organometallic clusters, previously synthesized or non-existent, have provided useful results in the context of organometallic ruthenium NPs [3]. We have more particularly focused on the ^{1}H NMR properties of these compounds and established a link between electron-deficiency and low-field resonance of hydrides adsorbed at the surface of Ru clusters or NPs. From a more general point of view, ^{1}H NMR and ^{2}H MAS-NMR techniques are of high

practical importance for characterizing the presence of hydrides (or deuterides) in ruthenium clusters and nanoparticles [4–6]. According to the work done in our group in the specific context of Ru clusters and mononuclear complexes, DFT calculations of chemical shielding tensors (σ) as well as electric field gradient (EFG) tensors seem accurate [3, 7, 8]. However, one should pay attention that owing to the NMR timescale, ^{1}H and ^{2}H NMR properties are highly dependent of the motion of hydrides in organometallic complexes or at the surface of Ru NPs. EFG calculations in Ref. [8] were mainly compared to low-temperature MAS-NMR data which were considered close to the so-called rigid limit, but such experiments are not so easy to achieve [9]. At sufficiently high temperature, proton spectra of fluxional compounds consist in the superposition of several bonding situations. A relevant, but computationally expensive, way to take into account the motion of protons consists in performing molecular dynamics (MD) simulations at the ab initio or DFT level of theory and to average the theoretical spectroscopic data [10–12]. We have developed in our group a Car–Parrinello MD (CPMD) code using atom-centered basis functions, which is a tool of choice for taking into account the role of temperature on the motion of nuclei [13, 14], and to calculate several properties with quantum chemistry methods more familiar to theoretical chemists. The importance of the Berry pseudorotation process in the interpretation of the ^{19}F NMR spectrum of phosphorus pentafluoride (PF_5) has been shown in Ref. [11]. Ab initio MD (AIMD) simulations have been performed to generate a large number of geometries considered for NMR parameter computations at the DFT level. It has been shown that averaged ^{19}F chemical shifts and spin–spin coupling constants calculated for the five fluorine atoms converge towards the NMR equivalence of the five atoms when the Berry pseudorotation mechanism is accounted for. Although AIMD can also be applied to larger systems, there is a need for lowering the cost of quantum chemistry calculations. It is the purpose of effective group potentials (EGPs), which aim at simplifying molecular ab initio calculations for large systems involving bulky ligands as long as these ligands can be supposed to play the role of spectator groups. In an EGP, a group of atoms is replaced by one or several fictitious atoms associated with energy levels and orbitals necessary for representing the active/spectator bond(s), in conjunction with a mono- or multi-centered pseudopotential. The principle of molecular pseudopotentials was briefly reported by Durand and Malrieu in 1987 [15]. Primary developments and promising tests were carried out in the Toulouse group in the late 1980s, but were not published since the transferability of this new tool was not obvious. This was the prolegomena to EGPs in Toulouse. EGPs witnessed a renaissance in the late 1990s and have been extensively developed and used in their present formulation. They are hereafter considered as the first generation of EGPs. Their definition and the way to derive their parameters have been in particular given in Ref. [16]. The accuracy and limitations of this tool has been discussed in several papers, mainly devoted to organometallic compounds [17–20] and its usefulness in terms of solution to the link atom problem has also been considered [21]. A summary of the cons and pros of EGPs has temporarily ended this successful attempt to reduce the computational time by reducing both the number of electrons and nuclei explicitly treated in ab initio calculations [22]. The reader interested with an overview of the miscellaneous propositions of molecular pseudopotentials is suggested to read the introduction of the article of Slavíček and Martínez [23], which introduces a multicentered valence electron effective potential description of functional groups which also succeeds in the context of excited electronic states. Note also the interesting proposition to modify carbon ECPs for substituted cyclopentadienide ring carbons for use in QM/MM calculations [24].

The main purposes of this article are first to provide new directions for the derivation of multicentered EGPs and second to show that AIMD simulations can take advantage of the reduction of the cost involved by EGPs, owing to some limitations, which should be overcome in the next generation of these molecular pseudopotentials. New results for a tetrahedral ruthenium cluster, namely $Ru_4Ar^{\#}_4H_4$ (where $Ar^{\#}$ stands for a pseudo η^6-C_6H_6 ligand), are also provided as well as a joint EGP/ab initio MD study aiming at finding free energies of activation in a *bis*-cyclopentadienyl lanthanide complex.

2 Effective group potentials

2.1 The case of η^6-C_6H_6 ligands

The construction of an EGP first requires to identify the characteristics of the target functional group from simple MO theory. An η^6-C_6H_6 ligand is considered as a 6 π-electrons system. Metal–ligand interactions will essentially involve π (shown in Fig. 1a), and possibly π^*, MOs of benzene and the symmetry-relevant AOs of the metal. EGPs considered in this section will be extracted in that context. Although σ and π MOs are not well separated in energy (actually the highest occupied σ MOs lie above the lowest occupied π MOs), σ MOs are not considered due to a weak overlap with the metal AOs [25].

The basic methodology underlying the derivation of EGPs, rather simple, has been described in Ref. [16] and recalled in Refs. [21] and [22]. Although it will not be explained in details in the present paper, some guidelines are necessary in order to present new ideas which could

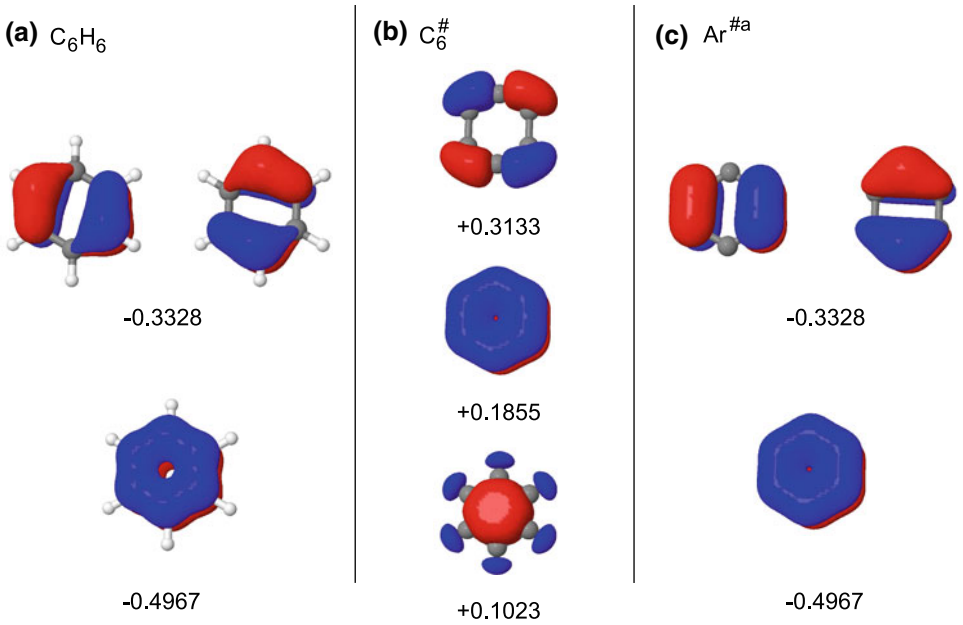

Fig. 1 Design of an η^6-C_6H_6 EGP **a** Reference HF π MOs in the 6-31G(*d,p*) basis set; **b** HF MOs obtained in the minimal truncated basis (i.e. one *p* GTO/$C^{\#}$ atom, see Sect. 2.1), with carbon ECPs in order to take into account the repulsion of the 1*s* core, but without the non-local part of $\hat{W}_{EGP}$ (i.e. without $\sum\sum \alpha_{nm}|g_n\rangle\langle g_m|$); **c** HF π MOs obtained with EGP_a. The MO energies are given in hartree

serve as a basis for deriving new multicentered molecular pseudopotentials. The role of EGPs is to remove some of the electrons and nuclei of functional groups which are considered as inactive, or spectators. This is done in two indivisible steps, achieved in the context of the Hartree–Fock (HF) method and based on reference calculations performed on benzene, in a large basis set $\{\chi_p\}$ of Gaussian-Type orbitals (GTOs, namely a polarized double-zeta basis set in the present case):

1. *The definition of a fictitious chemical group*, with a reduced number of electrons and nuclei. An η^6-C_6H_6 ligand is substituted by an hexagonal system with six pseudo-carbon atoms $C^{\#}$ which occupy the position of the actual carbon atoms in benzene. Each $C^{\#}$ atom brings a single electron in a *p* atomic orbital (AO), in order to describe the three occupied π MOs ϕ_i of benzene, which define the minimal set of active orbitals of this functional group ($N_{act} = 3$, see Fig. 1a). We have already checked that this minimal truncated basis set $\{f_q\}$ is sufficient for a proper description of the ligand–metal bonding. The exponent of the truncated GTO basis set $\{f_q\}$ is done in order to obtain the best molecular valence pseudo-orbitals (MVPOs), that is pseudo-MOs ϕ_i^{ps} built in this truncated basis set which are as close as possible to the N_{act} active molecular orbitals of the real system [16]. This step, analogous to the definition of valence pseudo-orbitals in the shape consistent version in the effective core potentials (ECPs) determination [26, 27], involves *de facto* a σ/π separation. Note that the optimized exponent for benzene (ζ_p: 0.332) is very close to the exponent optimized [19] for η^5-C_5H_5 (ζ_p: 0.312), thus suggesting that a unique exponent could be considered for carbon atoms involved in aromatic compounds coordinated by their π electrons. The pitfall of the drastic simplification introduced in this first step lies in the fact that such calculations are done in the context of Self-Consistent-Field (SCF) methods and not extended-Hückel or tight-binding calculations. As a consequence, although the actual ligand and its $C_6^{\#}$ counterpart are expected to be isolobal analogues according to the definition given by Hoffmann [28], the SCF process is ruled by the optimal stabilization of the $C_6^{\#}$ system. It is shown in Fig. 1b that the energies and shapes of the three actual HF MOs of $C_6^{\#}$ are far from the A_{2u} and E_g π MOs of benzene. The lowest one consists in a bonding symmetric σ MO built from radial *p* AOs. The second one is the expected totally bonding A_{2u} π MO, but it lies 18 eV above its C_6H_6 counterpart. The third one is a σ bonding MO which exhibits two nodal planes. They are far from the target π MOs of an η^6-benzene ligand, both in terms of shape and energy. It it thus mandatory to introduce an operator in the hamiltonian in order to obtain at the end of the SCF process the relevant active MOs of the functional group. If one defines $\hat{F}^{ref}$ and $\hat{F}^{\#}$ as the Fock operators of the reference and model systems, respectively, the operator which should be added to $\hat{F}^{\#}$ is the exact $\hat{F}_{EGP}$ operator. This operator is obviously molecule-dependent and not transferable to other systems. It is the reason why we hereafter introduce a transferable operator, namely $\hat{W}_{EGP}$ (see Refs. [16] or [21] for more details).
2. *The definition of an operator associated to the fictitious chemical group*, hereafter called $\hat{W}_{EGP}$, which

will compel the SCF process to converge on three π MOs which must be as close as possible to those of the real chemical group in terms of shape and energy. The main part of this molecular pseudopotential is formulated with a non-local form ($\sum\sum \alpha_{nm}|g_n\rangle\langle g_m|$), which presents some numerical advantages [29] and which ensures its transferability [16]:

$$\hat{W}_{\mathrm{EGP}} = \sum_n \sum_m \alpha_{nm}|g_n\rangle\langle g_m| - \sum_{i=1}^{n_\#} \frac{Z_i^{\mathrm{eff}}}{r} + \sum_{i=1}^{n_\#} \hat{W}_{\mathrm{ps}}(i) \qquad (1)$$

where $n_\#$ is the total number of fictitious atoms, the functions $|g_n\rangle$ are gaussians functions with predetermined exponents, and $\hat{W}_{\mathrm{ps}}(i)$ is the ECP of the real atom. The advantage of this ECP is to already take into account, if necessary, the repulsion of core electrons, although repulsion could have been included as a criterion to be fulfilled by the non-local part of $\hat{W}_{\mathrm{EGP}}$ (in that case, $\hat{W}_{\mathrm{EGP}}$ would be reduced to the sum of the non-local part and the Coulomb term). Thus the calculation of the EGP operator in a GTO basis set is obtained by simple products of gaussian overlaps, in addition to the integrals of the Coulomb and ECP terms which are available in standard quantum chemistry packages. The exponents of the g_n functions are chosen so that two conditions are simultaneously fulfilled: (a) the isolobal analogy between the active MOs of the real functional group and the SCF MOs of the fictitious group; (b) $\hat{W}_{\mathrm{EGP}}$ must be a short-range operator since it must only act on the electrons of the spectator chemical group which are kept. Similarly to the cyclopentadienyl case, the operator basis set has been firstly defined as an even-tempered basis set of *p*-type gaussian functions, with the exponents 3, 1.5, 0.75 and 0.375. The parameters α_{nm} are obtained by a least-squares fit method proposed in 1980 by Nicolas and Durand [30] (so far other EGPs will be considered in the following, the non-local part of $\hat{W}_{\mathrm{EGP}}$ fitted with this basis set will hereafter be called EGP_a). The mathematical form of the non-local part of $\hat{W}_{\mathrm{EGP}}$ is very general, and there is no a priori introduction of σ or π parts in the multinuclear core. In principle, that is in the favorable case of a large number of information defining the reference system, in conjunction with a wide basis set $\{g_n\}$, the least-squares fit method of Nicolas and Durand should automatically provide the most important $|g_n\rangle\langle g_m|$ terms, i.e. with the largest α_{nm} parameters. We will see later that EGPs are rather generated in the context of a small number of information, which may involves numerical instability.

The truncated GTO basis set, the effective charge $Z^{\mathrm{eff}} = 1$ for each $C^\#$ atom, the operator basis set $|g_n\rangle$ and the parameters α_{nm} of this operator completely define the pseudo η^6-C_6H_6, which will be hereafter called $Ar^{\#a}$. The three SCF π MOs of $Ar^{\#a}$, shown in Fig. 1c, shed light on the good behavior of the $\hat{W}_{\mathrm{EGP}}$ operator. However, one should pay attention that systematic tests must be done in order to check the accuracy and transferability of any new EGP, owing to some numerical instability of the least-squares fit method. The limitation of this method will be commented on in the next section.

The EGP routines have been implemented in the Gaussian03 package [31]. During geometry optimizations, the distance between the chemical group replaced by an EGP and the active part is kept fixed at a standard value.

2.2 Discussion about the pseudopotential and new prospects

As already commented in Ref. [21], the least-squares fit method used for the determination of optimized α_{nm} parameters may yield chemically irrelevant results albeit the norm is close to zero. This is related to the rather poor sample of information considered in the least-squares fit process, i.e. a $N_{\mathrm{act}} \times N_{\mathrm{act}}$ Fock operator, (so far $N_{\mathrm{act}} = 3$ for η^6-C_6H_6). A solution to avoid this artefactual procedure would be to increase the number of information to be fit. Note that in the shape-consistent extraction of atomic pseudopotentials, the condition imposed to fit the parameters of the pseudopotential is $\hat{F}_{\mathrm{ps}}\varphi_i^{\mathrm{ps}} = \varepsilon_i\varphi_i^{\mathrm{ps}}$, where ε_i is the energy of the real valence AO φ_i and φ_i^{ps} is the valence pseudo-orbital which fits φ_i in the valence region. The specification of $\varphi_i^{\mathrm{ps}}(r)$ for any value of r provides enough information to fix $\hat{W}_{\mathrm{ps}}$. In the energy-consistent approach [32], $\hat{F}_{\mathrm{ps}}\varphi_i^{\mathrm{ps}} = \varepsilon_i\varphi_i^{\mathrm{ps}}$ is solved not only for the electronic ground state, but also for electronic excited states, $\hat{W}_{\mathrm{ps}}$ being determined in order to fit the energy difference between these states. Note that extraction of EGPs could take advantage of the energy-consistent approach used for defining ECPs. Unfortunately, the method proposed by Nicolas and Durand is not free of numerical instability. We shall now propose a new way to perform the second step of the EGP extraction process. For that, we shall first try to answer the following question: what is the shape of an EGP ? While ECPs on one hand or quantum capping potentials proposed as link atoms in QM/MM methods [33, 34] on the other hand have a repulsive shape, easily shown by the plot of $\hat{W}_{\mathrm{ps}}(r)$, it is less straightforward to visualize the nature of $\hat{W}_{\mathrm{EGP}}$. A way to more deeply understand the role of this molecular pseudopotential is to formulate the non-local part of the operator ($\hat{W}_{EGP}^{NL}$) in a diagonal form:

$$\hat{W}_{\mathrm{EGP}} = \sum_{I=1}^{N_{\mathrm{EGP}}} \Lambda_I|G_I\rangle\langle G_I| - \sum_{i=1}^{n_\#} \frac{Z_i^{\mathrm{eff}}}{r} + \sum_{i=1}^{n_\#} \hat{W}_{\mathrm{ps}}(i) \qquad (2)$$

$$= \hat{W}_{\mathrm{EGP}}^{\mathrm{NL}} - \sum_{i=1}^{n_\#} \frac{Z_i^{\mathrm{eff}}}{r} + \sum_{i=1}^{n_\#} \hat{W}_{\mathrm{ps}}(i) \qquad (3)$$

where Λ_I and $|G_I\rangle$ are the eigenvalues and eigenvectors of the α_{nm} matrix. Each eigenvector $|G_I\rangle$ is a linear

combination of the N_{EGP} gaussian functions which define the basis set of $\hat{W}_{\mathrm{EGP}}$:

$$|G_I\rangle = \sum_{n=1}^{N_{\mathrm{EGP}}} c_{In}|g_n\rangle \tag{4}$$

$\hat{W}_{\mathrm{EGP}}$ is thus a finite sum of projectors $|G_I\rangle\langle G_I|$ with weights Λ_I, in addition to Coulomb and ECP operators (Fig. 2).

In the case of $\mathrm{EGP_a}$, the dimension of the operator basis set is $N_{\mathrm{EGP}} = 72$, with four p-type gaussian functions per atom. Among the 72 eigenvectors of the α_{nm} matrix, only 24 actually play a role in the total hamiltonian since the eigenvalues Λ_I of the 48 other eigenvectors cancel. One can however raise doubts on the interest of 21 of the 24 remaining eigenvectors, since the absolute value of the associated eigenvalues are smaller than 0.1 hartree, whereas the three main components of the non-local part of $\hat{W}_{\mathrm{EGP}}$ are close to -0.7 hartree. These three eigenvectors, namely $|G_1\rangle$, $|G_2\rangle$ and $|G_3\rangle$, are plotted in Fig. 3. The striking similarity between the main components of $\hat{W}_{\mathrm{EGP}}^{\mathrm{NL}}$ and the three active π MOs of benzene sheds a new light on the role of EGPs. $\hat{W}_{\mathrm{EGP}}^{\mathrm{NL}}$ is nothing else than a level-shift operator which aims at stabilizing the active MOs. In the present case, the weights $\Lambda_{1\text{-}3}$ are of the order of magnitude of the energy difference between the real MOs ϕ_i and the SCF MOs of $C_6^{\#}$ calculated in the truncated basis set. Nevertheless, Λ_I parameters strongly depend on the spatial extension of the operator basis set, namely $\{g_n\}$. The less diffuse the basis set, the larger the absolute values of the weights Λ_I. Although in the present development $\hat{W}_{\mathrm{EGP}}^{\mathrm{NL}}$ only acts in order to stabilize the active occupied MOs in the SCF process, the active set of MOs could easily be extended, for example to virtual MOs in order to suitably fix back-donation effects, such as for the carbonyl ligand [20]. This analysis suggests that the least-squares fit of Nicolas and Durand could be replaced by a new method for optimizing the parameters of $\hat{W}_{\mathrm{EGP}}^{\mathrm{NL}}$, by directly expressing this operator as a finite sum of projectors. It involves to tune N_{act} Λ_I weights, where N_{act} is the number of active MOs (6 or 3 in the case of benzene, whether π^* MOs are taken into account or not), instead of optimizing N_{EGP} parameters α_{nm} (72 in the case of $\mathrm{EGP_a}$). The lack of information at the origin of the numerical instability of the Nicolas and Durand fit could thus be solved. Step 2 would now be replaced by the following approach:

1. fix predetermined exponents for the basis set $\{g_n\}$ which defines $\hat{W}_{\mathrm{EGP}}^{\mathrm{NL}}$
2. find normalized functions G_I as close as possible to the N_{act} reference MOs ϕ_i. It can be done in the same spirit than the determination of the MVPOs, which are as close as possible to the reference MOs, but which are expressed in the truncated basis set $\{f_q\}$. The G_I would be obtained in two steps:

   (a) calculate the elements of the S matrix:

   $$S_{nm} = \sum_{i=1}^{N_{\mathrm{act}}} \langle g_n|\phi_i\rangle\langle\phi_i|g_m\rangle \quad n,m = 1,N_{\mathrm{EGP}} \tag{5}$$

   (b) diagonalize S and select the N_{act} eigenvectors with eigenvalues closest to 1.

3. optimize the weights Λ_I at the same time so that the energies and shapes of the active MOs are well reproduced

This proposition will be evaluated in a forthcoming paper.

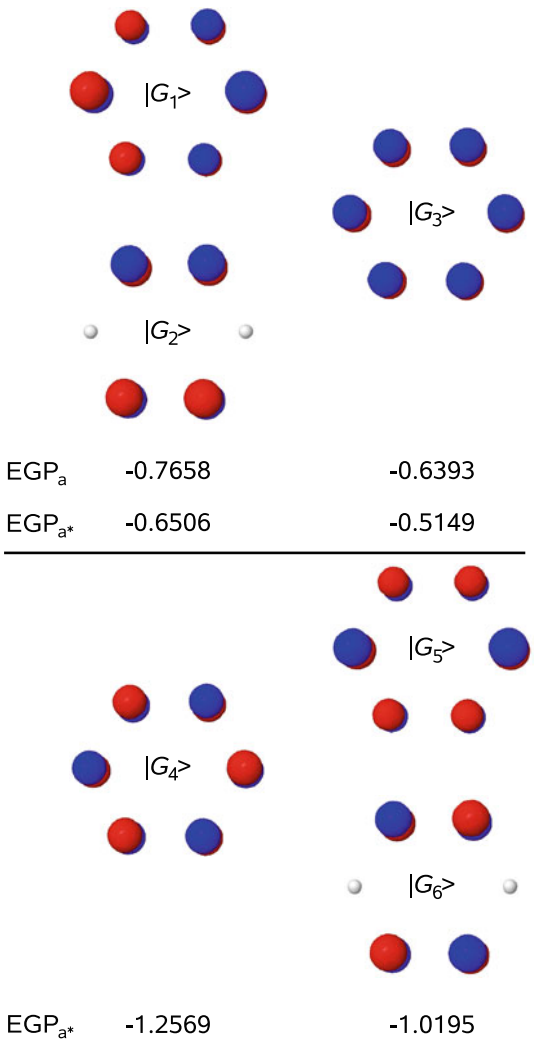

Fig. 2 Graphical representation of the main terms $|G_I\rangle$ of $\hat{W}_{\mathrm{EGP}}^{\mathrm{NL}}$ operators. $\mathrm{EGP_a}$ and $\mathrm{EGP_{a^*}}$ are respectively defined by $|G_{1\text{–}3}\rangle$ and $|G_{1\text{–}6}\rangle$. The weights Λ_I (in hartree) are given below for each EGP

2.3 The η^6-C_6H_6 EGP: a useful tool in the context of organometallic nanoparticles?

The accurate calculation by means of molecular quantum chemistry methods of the geometric and spectroscopic properties of organometallic NPs is desirable, but for the time being, it requires appropriate simplifications. One of them could be supplied by EGPs, in the context of molecular quantum chemistry. Small organometallic clusters are useful in order to validate this suggestion, such as the ruthenium clusters recently investigated in our group [3]. We will consider now benzene ruthenium clusters, which also exhibit hydrido ligands. The water-soluble tetranuclear ruthenium cluster $[(H)_4Ru_4(C_6H_6)_4]^{2+}$, synthesized for the first time in 1994 [35], is an electron-deficient species (58e) according to electron-counting rules [25, 36, 37]. Additional joint experimental and theoretical works on $[(H)_4Ru_4(C_6H_6)_4]^{2+}$ showed a small energy gap between the ground state which turned out to be a diamagnetic singlet state (S_0) and the first excited paramagnetic triplet state (T_1) [38]. In agreement with that previous work, we have recently confirmed that the triplet state lies 3.8 kcal mol^{-1} above the singlet state [3]. The $(H)_4Ru_4(C_6H_6)_4$ molecule has a T_d symmetry, in relation with the optimal number of electrons of this *nido* species (60e). The four hydrides are bonded as symmetrical μ_3 caps above the triangular faces of the Ru_4 core, whereas the benzene ligands are coordinated to the ruthenium centers via their π electrons. The $Ar^{\#}$-substituted compound is shown in Fig. 3.

For a 60e tetrahedral cluster such as $(H)_4Ru_4(C_6H_6)_4$, the electronic ground state is defined by the occupation of ligands and metal–ligands MOs, four Ru–H MOs, six skeletal Ru–Ru MOs and eight metal–metal MOs which have mainly non-bonding character. We have considered several EGPs, which differ by the basis set which define $\hat{W}_{EGP}^{NL}$: EGP_a, EGP_b and EGP_c are all built according to four *p*-type gaussian functions, EGP_a (ζ: 3.0, 1.5, 0.75, 0.375) being more diffuse than EGP_c (ζ: 12.0, 6.0, 3.0, 1.5), EGP_b being in-between (ζ: 6.0, 3.0, 1.5, 0.75). EGP_a is extracted in the same basis set than the cyclopentadienyl EGP, which turned out to be accurate [19]. It does not exhibit similar qualities in the case of η^6-benzene ligands, since the DFT calculation applied on the optimal geometry of the reference structure calculated in Ref. [3] did not converge. EGP_b and EGP_c did slightly better, but the SCF process failed to converge at the second step of the optimization process. EGP_c, a short range operator, performs better, but it yields poorly accurate geometries. Although the metal–hydrogen distance is close to the reference value (1.82 Å vs. 1.83 Å), the metal–metal distances are smaller than the reference calculation by 0.14 Å (2.63 vs. 2.77 Å). The last pseudopotential, namely EGP_d, is built in a larger basis set which spreads from 12.0 to 0.375. It also failed at the second step of the optimization process.

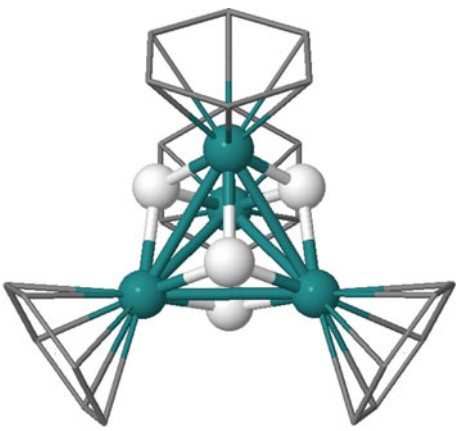

Fig. 3 Tetrahedral $Ru_4Ar^{\#}_4(\mu_3{-}H)_4$ cluster

This new multicentered EGP is disappointing, whereas according to the previous work on a pseudo-C_5H_5 it was expected to fairly behave. The main difference between cyclopentadienyl and benzene is the lowest HOMO-LUMO energy gap in the case of C_6H_6, which involves a more important π^* back-donation in metal–benzene bonding. Four additional EGPs have been extracted, defined by the same basis sets than $EGP_{a–d}$. A simultaneous fit of the shape and energies of the three highest π MOs and of the three lowest π^* MOs has been imposed. EGP_{a*-d*} all accurately reproduce the π^* MOs energies ($\varepsilon^* = 0.1353 \times 2, 0.3482$) and shapes. As can be seen in Table 1, no convergence failure did occur in the case of $(H)_4Ru_4Ar^{\#}_4$, thus showing the necessity to suitably describe back-bonding effects in such compounds. The most accurate Ru-Ru bond length is found with EGP_{a*}, the benzene counterpart of the EGP developed for cyclopentadienyl in Ref. [19], with special attention paid to virtual π* MOs in the case of C_6H_6. However, the Ru–H bond length is slightly overestimated by 0.044 Å. EGP_{c*}, the short-range operator, is the less accurate since the Ru–Ru bond length is underestimated by 0.104Å, although on the other hand the Ru–H bond length is incidentally identical to the reference value. EGP_{d*}, whose operator spreads on the widest range, performs fairly well, with the Ru–Ru distance smallest than the reference value by 0.019 Å, whereas the Ru–H distance is overestimated by 0.029 Å. Energy-levels diagrams of the occupied MOs close to the Fermi level are reported in Fig. 4. On the contrary to $EGP_{a–d}$, the t_1 and *e* skeletal Ru–Ru MOs lie below the most stable t_2 non-bonding metal MO, in agreement with the reference calculation. The energy differences between all MOs of $(H)_4Ru_4Ar^{\#}_4$ obtained with $EGP_{a*–d*}$ are in excellent agreement with those of $(H)_4Ru_4(C_6H_6)_4$. The main apparent discrepancy is a systematic shift between the energies of the reference and pseudo molecular systems, probably related to the insufficient shielding of the $\hat{W}_{EGP}$

Table 1 Comparison of the properties of $[(H)_4Ru_4(C_6H_6)_4]^{n+}$ and $[(H)_4Ru_4Ar^{\#}_4]^{n+}$ (n = 0 or 2) for EGP defined according to occupied and lowest unoccupied π MOs ($EGP_{a^*\text{-}d^*}$)

	$[(H)_4Ru_4(C_6H_6)_4]^{n+}$	$[(H)_4Ru_4Ar^{\#}_4]^{n+}$			
		EGP_{a^*}	EGP_{b^*}	EGP_{c^*}	EGP_{d^*}
$n = 0$, ground state (T_d)					
R_{RuRu}	2.77	2.76	2.72	2.66	2.75
R_{RuH}	1.83	1.87	1.84	1.83	1.86
$n = 2$, singlet state S_0 (C_S)					
R_{RuRu}	2.84 × 4	2.85 × 4	2.79 × 4	2.74 × 4	2.83 × 4
	2.59 × 2	2.60 × 2	2.55 × 2	2.50 × 2	2.58 × 2
R^{a}_{RuH}	1.84 × 2	1.89 × 2	1.87 × 2	1.87 × 2	1.88 × 2
	1.89	1.90	1.88	1.84	1.89
$n = 2$, triplet state $T_1(\sim C_{3v})$					
R_{RuRu}	2.75 × 6	2.77 × 6	2.71 × 6	2.65 × 6	2.75 × 6
R_{RuH}	1.85 × 3	1.89 × 3	1.87 × 3	1.85 × 3	1.88 × 3
$n = 2$, ΔE_{ST}	3.8	4.8	2.8	1.0	3.8

Distances in Å, energy differences in kcal mol^{-1}

Severe numerical instabilities have been observed for most EGPs built by taking into account occupied π MOs only. EGP_a: SCF not converged, EGP_b and EGP_d: geometry optimization not converged, EGP_c: R_{RuRu} 2.63 Å and R_{RuH} 1.82 Å

[a] Averaged values

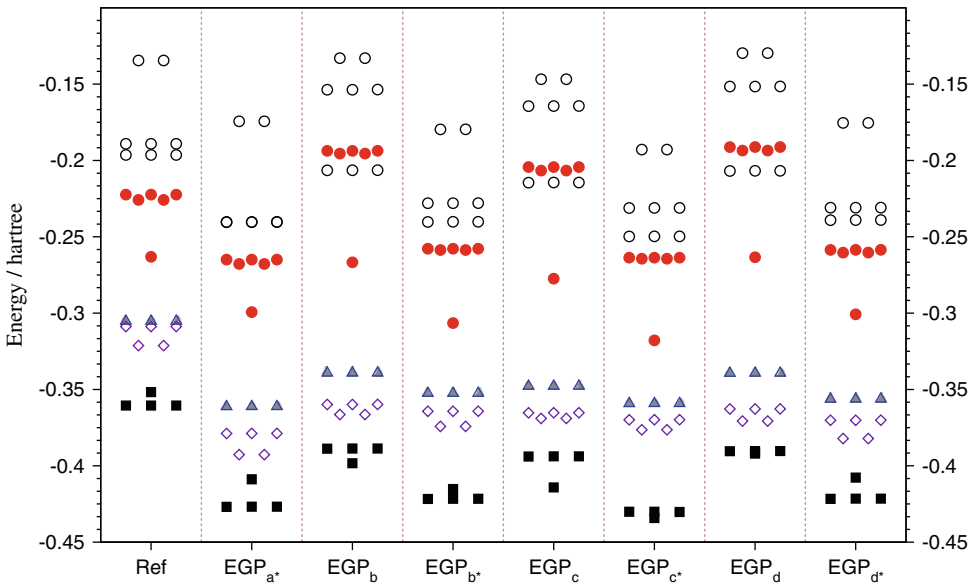

Fig. 4 Energy-level diagrams of the occupied MOs of $(H)_4Ru_4(C_6H_6)_4$ and $(H)_4Ru_4Ar^{\#}_4$ close to the Fermi level, calculated for the optimal geometry of $(H)_4Ru_4(C_6H_6)_4$. *open circle* non-bonding or weakly bonding Ru–Ru MOs (E and T_2 symmetry); *filled circle* skeletal Ru_4 MOs (T_1, E and A_1 symmetry); *filled triangle* C_6H_6 or $Ar^{\#}$ MOs; *open diamond* C_6H_6−Ru or $Ar^{\#}$−*Ru* MOs; *filled square* Ru–H MOs (A_1 and T_2 symmetry)

operator. Note that it could be possible to add repulsion by an appropriate parametrization of conventional effective core potentials [33, 34].

The shape of some selected MOs, namely the six skeletal (or metal-metal) MOs and the four metal–hydrogen MOs are shown in Fig. 5. As already observed in the case of benzene, there is a remarkable similarity between the reference MOs of $(H)_4Ru_4(C_6H_6)_4$ and the MOs of $(H)_4Ru_4Ar^{\#d^*}_4$, with the exception of the triply degenerate Ru–H MOs. While the totally symmetric Ru–H MO of $(H)_4Ru_4Ar^{\#}_4$ is almost identical to the corresponding MO in $(H)_4Ru_4(C_6H_6)_4$, the three other MOs of the model system do not match the reference MOs due do a slight mixing of the Ru_4H_4 fragment MOs with σ MOs of the $(C_6H_6)_4$ fragment. It is not possible to obtain such mixing, since $\sigma(C_6H_6)$ MOs cannot be described by an $Ar^{\#}$ EGP. The energy difference between the Ru–H MOs in $(H)_4Ru_4Ar^{\#}_4$ is nevertheless analogous to $(H)_4Ru_4(C_6H_6)_4$, owing to the small $\sigma(C_6H_6)$ contribution. The energies and shapes of the MOs as well as the geometrical properties of the tetrahedral Ru_4 cluster show that most of the η^6-C_6H_6 EGPs are able to create an accurate ligand field around the Ru_4H_4 moiety.

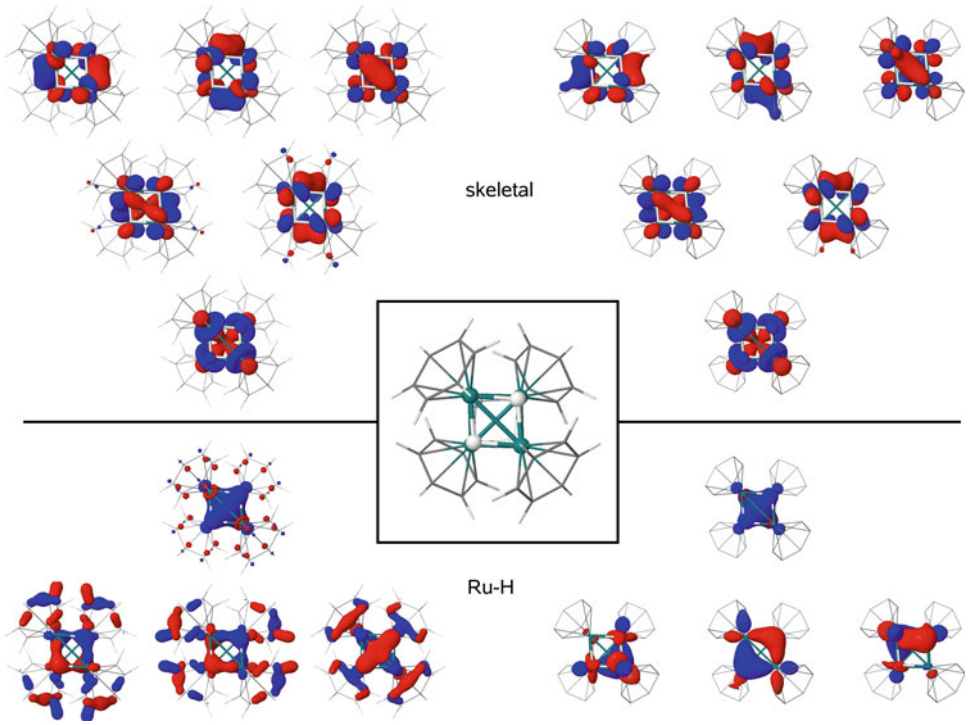

Fig. 5 Comparison of the skeletal (T_1, E and A_1 symmetry) and Ru-H (A_1 and T_2 symmetry) MOs of $(H)_4Ru_4(C_6H_6)_4$ and $(H)_4Ru_4Ar_4^{\#d^*}$, with $Ar^{\#d^*}$ = 1*p* per $C^{\#}$ ($\zeta = 0.332$) + EGP_{d^*}

The $[(H)_4Ru_4(C_6H_6)_4]^{2+}$ compound is a more tricky system, with the lowest electronic triplet state T_1 which lies only 3.8 kcal mol^{-1} above the singlet ground state S_0. As can be seen in Table 1, all EGPs extracted from occupied and virtual π MOs of benzene, namely $EGP_{a^*-d^*}$, perform well, both in terms of geometry and singlet–triplet energy difference (ΔE_{ST}). EGP_{a^*} and EGP_{d^*} are the most accurate, whereas ΔE_{ST} as well as Ru–Ru bond lengths are underestimated with EGP_{c^*}. As already mentioned, that short-range EGP is the less reliable. However, it behaves better than a fifth EGP, which spans a more diffuse space (EGP_{e^*}, ζ: 3.0, 1.5, 0.75, 0.375, 0.1875, 0.09375). The diffuse functions are probably responsible of the attractive character of this EGP, which manifests itself by the optimal geometry of $[(H)_4Ru_4Ar_4^{\#e^*}]^{2+}$, with two edge-bridging H and two terminal-H instead of four face-capping H atoms. Each hydride in top position is located very close to an $Ar^{\#}$ fragment. ΔE_{ST}, found to be 216 kcal mol^{-1} (!), is also an indication of the unreliability of this EGP. It confirms that long-range $\hat{W}_{EGP}^{NL}$ operators act both on the fictitious part and unexpectedly on the active part close to the active/spectator boundary.

3 A joint EGP/molecular dynamics study

3.1 Ab initio molecular dynamics

From a quantum chemical point of view, the characteristic values of a physico-chemical reaction are obtained from the knowledge of specific point on the potential energy surface associated to the process. In most cases, kinetic or thermodynamic data are determined using calculated Gibbs free energies for which the entropic contributions are estimated using the harmonic approximation [39]. In some cases, this harmonic approximation leads to results in poor agreement with experimental knowledge, since anharmonic contributions must be taken into account. This can be performed as a correction of harmonic approximation and is implemented in most standard quantum chemical codes [40]. Another way to explore potential energy surface and to estimate the temperature effect added to electronic energies is based on a dynamical approach. In this specific case, temperature is explicitly controlled by simulating the canonical ensemble by means of thermostats [41] in a molecular dynamics simulation scheme. The thermodynamic and kinetic data can then be determined by employing a constraint [42] that must correspond to the reaction coordinate.

Molecular dynamic simulations were initially based on empirical interaction potentials determined from experimental data. Since the appearance of the Car–Parrinello molecular dynamics technique [43], more general molecular dynamics approaches have known a tremendous development both from an application and development point of view. Rather than using empirical interaction potentials, the electronic energy and the forces on nuclei that are necessary to resolve Newton classical equations of propagation are computed by wavefunction-based or density-based methods. Mainly two types of molecular

dynamics schemes can be highlighted: the so-called Born–Oppenheimer [44–47] and Car–Parrinello molecular dynamics techniques. In the first case, the electronic energy and its associated nuclear derivatives are calculated after an energy minimization procedure that must be fulfilled at each step of the molecular dynamic simulation. This procedure is necessary in order to obtain stable behavior of the molecular dynamics simulation relative to the molecular system total energy for long time propagation. In the case of Car–Parrinello molecular dynamics, a new degree of freedom is introduced, namely the wavefunction. Consequently, the nuclear degrees of freedom and the wavefunction evolve according to the Newton law and the SCF convergence procedure can be avoided.

It must be noted that most of the Car–Parrinello algorithms are based on the density functional theory (DFT) approach coupled with a plane wave basis set description of the electronic structure. While this approach presents many advantages, the use of plane waves may be ill-suited for the study of non-periodic chemical systems and to describe cusps and high electronic inhomogeneities. Consequently, following the initial proposition of Carter [48, 49], we have developed a few years ago an algorithm based on Car–Parrinello Lagrangian but using atom centered basis functions (more precisely Gaussian type basis sets) for the electronic structure calculation part of the procedure [13]. This algorithm has been coupled with several tools in order to improve our way to explore chemical reaction and physico-chemical processes. For instance, Nosé-Hoover chain of thermostats [41, 50] have been implemented in our molecular dynamics code in order to perform molecular dynamic simulations at finite temperature. This specific tool has allowed to explore molecular dynamic treatment of Infra-Red [51–53], NMR [11] and UV [12] spectroscopic properties. Moreover, in order to explore chemical reactivity, it has been necessary to introduce a statistical mechanical procedure that samples the phase space along a defined reaction coordinate and allows the estimation of relative free energies (i.e. free energy barriers of a chemical process). In this context, two types of chemical reaction have been studied [14, 54]. These studies have permitted to demonstrate the failure of the "static" approach based on the harmonic approximation used for Gibbs free energy calculations in the case of flat potential energy surfaces.

3.2 Reactivity of a lanthanocene complex: a test case

3.2.1 *Motivations*

Lanthanide chemistry has witnessed an increasing interest over the last three decades. In particular, Watson and Parshall have shown that Cp^*_2LuH ($Cp^* = C_5Me_5$) or Cp^*_2LuMe can react rapidly with H_2 [55]. This reaction is a prototype of reactions in lanthanide chemistry, extensively studied by quantum chemistry methods [56, 57]. Theoretical studies have been extended for the activation of other bonds (C–H, C–F, Si–H, etc.), leading to successful experimental and computational works [58–60]. Quantum chemistry can indeed provide very relevant insights on multi-step reactions. However such studies are generally restricted to the search of stationary points on potential energy surfaces. Although MD simulations could bring additional information, the study of chemical reactions by AIMD is still a challenge. The CPMD method has however been applied to study the hydrogen exchange catalyzed by a lanthanocene complex [14]. In this study both cyclopentadienyl rings have been substituted by chloride ligands in order to reduce the computational cost, taking advantage of the fair isolobality of Cp and Cl ligands. Interestingly, it has been shown that anharmonicity effects are of great importance for the evaluation of the activation barrier of this reaction and that the harmonic approximation which is usually used to estimate vibrational entropic contributions may fail.

EGPs could be very appropriate tools to efficiently model a spectator ligand and to drastically reduce the associated computational cost. It has already been recalled in Sect. 1 that the pseudo η_5-C_5H_5 EGP ($Cp^\#$) has successfully been used to mimic a real η_5-C_5H_5 cyclopentadienyl ligand [61]. For these previous reasons, we focus on an AIMD study of the hydrogen exchange reaction catalyzed by a Cp_2LaH complex, where two $Cp^\#$ EGPs fill in for the real Cp rings:

$$Cp^\#_2La{-}H^* + H{-}H \longrightarrow Cp^\#_2La{-}H + H^*{-}H.$$

3.2.2 *Evaluation of free energy activation barriers with AIMD*

In the case of free (i.e. non-constrained) ab initio molecular dynamics simulations, two important thermodynamic quantities for a chemical process, namely entropy and free energy, cannot in general be derived from a statistical average. These global properties depend on the extent of the phase space accessible to the molecular system during the simulation [39, 62]. The probability of finding the system in a transition state region is so small that, therefore, no relative free energies of a chemical process can be calculated by natural molecular dynamics simulation. Several statistical mechanical procedures circumvent this problem. For instance, the original "umbrella-sampling" method [63, 64], which adds a coordinate-dependent potential, leads to the system to sample a specific region of the phase space. Other approaches which are based on

similar ideas also allow the estimation of free energies for chemical processes, for instance the recent metadynamic methodology [65, 66] or the "blue-moon" method [67, 68]. The latter has been used to estimate free energy differences by sampling the phase space along a defined action pathway. By means of thermodynamic integration [62], free energy difference is obtained as:

$$\mathcal{F}(\xi_2) - \mathcal{F}(\xi_1) = \int_{\xi_1}^{\xi_2} \mathrm{d}\xi' \left\langle \frac{\partial \mathcal{H}}{\partial \xi} \right\rangle_{\xi'} \tag{6}$$

where $\mathcal{H}$ is the Hamiltonian of the system, $\xi(\mathbf{r})$ is a chosen reaction coordinate and $\langle \ldots \rangle_{\xi'}$ is an ensemble average at $\xi(\mathbf{r}) = \xi'$. This conditional average could be estimated by a time average over a constrained trajectory with the chosen reaction coordinate fixed at a specified value. Recently, generally applicable expressions for the average force of the constraint $f_\xi = -\nabla_\xi \mathcal{F}$, which is the opposite of the integrand in Eq. 6, have been outlined [42, 69]. It has been shown that the bias introduced by the constraint can be removed by considering the following expression:

$$f_\xi = \frac{\left\langle Z^{-1/2}(-\lambda + k_B T G) \right\rangle_\xi}{\left\langle Z^{-1/2} \right\rangle_\xi} \tag{7}$$

where k_B is the Boltzmann constant, T is the temperature, Z and G are, respectively, weight and correction factors, λ is the Lagrange multiplier of the associated holonomic constraint. Therefore, the obtained free energy differences might not be dependent on the choice of the constraint and accordingly to the Jarzynski inequality it leads to an upper bound for the activation barrier.

3.2.3 Computational details: potential energy calculations

Calculations were carried out at the DFT level of theory using the hybrid B3PW91 [70, 71] functional. A large core relativistic effective potential (ECP) optimized by the Stuttgart group and the corresponding basis sets have been used for the lanthanum center [72], whereas hydrogen atoms have been described with a 6-31G(*d,p*) double-ζ quality basis set [73]. The effect of Cp has thus been mimicked by the previously published EGP [19], five electrons are allowed to occupy the space spanned by *p* atomic orbitals ($\alpha = 0.312$) centered at the edges of the pentagonal ring. The computations of potential energy and the nuclear gradients have been carried out with the Gaussian 98 suite of programs modified to incorporate EGPs [74]. Free energy differences at room temperature have been estimated by means of the "Blue-Moon" approach.

CPMD simulations with Gaussian type orbitals have been performed with our own code [13]. Fictitious electronic mass was set to 170 a.u. and equations of motion have been integrated with a time step of 0.25 fs by means of a velocity Verlet scheme [75]. These simulations were performed in the canonical ensemble with Nosé–Hoover chains of thermostats [41] and holonomic constraints associated to the reaction coordinate have been applied considering the method of undetermined parameters. For each trajectory, a thermalization procedure has been performed for at least 6 ps, followed by a production simulation achieved for additional 5–6 ps. The property of interest, namely the force of the constraint, has been averaged as a function of time during the production step and its convergence has been checked at the end of the whole process.

3.2.4 Description of geometrical constraints

The choice of the constraint which represents the reaction coordinate can be a difficult task. Such constraint can be described by several geometrical parameters. Moreover, an incorrect choice of the type of constraint can induce a bias for free energy calculation. For the considered reaction, it is not obvious to find a function that will constrain the transition state geometry which can be mainly described by the concerted breaking and forming of four bonds. For this study, we have employed a well-tried type of constraint: it corresponds to the projection of the H^aH^b vector on the H^aH^c one (Fig. 6). This type of constraint has already been successfully applied for the hydrogen exchange catalyzed by Cl_2LaH [54].

3.2.5 AIMD linked with the EGPs

Ab initio molecular dynamics simulations can take advantage of the reduction of the cost involved by EGPs. On the other hand, the current formulation of EGPs (Eq. 1) does not include an explicit repulsive term in charge to mimic the screening effect of the inactive MOs of the real chemical group. As a consequence, the calculation of the gradient of the potential energy with respect to the position of each center which define a given $\hat{W}_{EGP}$ operator would be meaningless. This limitation binds the EGPs skeleton to be frozen during the molecular dynamics simulations. Moreover for the same reasons, atoms directly "bonded" to EGPs cannot be relaxed during a geometry optimization procedure, or allowed to move during a MD trajectory.

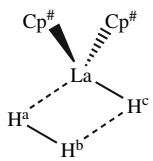

Fig. 6 Atom definition for the geometrical constraint

Consequently, only the positions of hydrogen atoms were allowed to evolve during the MD simulations and the geometrical structure of the $Cp^{\#}_2La$ fragment has been kept frozen. This leads to a modification for the number of degrees of freedom. Thus, the $Cp^{\#}_2La$ fragment could be seen as two fixed "rugby balls" linked by the top (Fig. 7). The H_3^- fragment is allowed to evolve in the field created by these associated rugby balls.

3.2.6 Conservation of the total energy

In order to illustrate the implementation of the approach discussed above, we focus our attention on the quality of the potential energy surface explored by the dynamics. In particular, the conservation of the total energy is carefully examined. One may note that the fictitious kinetic energy associated to the classical propagation of the Kohn-Sham orbitals in CPMD is not taken into account for the total energy. The latter includes the potential energy, the nuclear kinetic energy and the contributions of the Nosé–Hoover chain of thermostats.

One can suspect that the classical propagation of the Kohn–Sham orbitals by means of the Car–Parrinello procedure could be approximate, in particular in the transition state region where the concerted breaking and forming of four bonds occurs. The evolution of the relative total energy as a function of time for the trajectory which corresponds to the exploration of the transition state region ($\xi = 0.5$) is shown on Fig. 8. After 5 ps of simulation time, the total energy deviation is lower than 2×10^{-5} a.u. The range of CP dynamics' error for this trajectory remains below a very satisfactory limit. Moreover considering the employed integrator—a velocity Verlet scheme—and the integration time step—0.25 fs—this range of error is very close to the one expected for a reference Born–Oppenheimer MD simulation. The similar range of error has been measured for the trajectories performed for different values of the constraint ξ, which represents the reaction coordinate. Finally this satisfactory behavior and in particular the conservation of total energy leads us to be confident in the presented scheme, combining CPMD with GTO basis sets and EGPs.

3.2.7 Estimation of the free energy activation barrier

Using the previously discussed "blue-moon" method, the activation barrier has been estimated with a set of

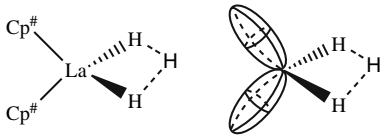

Fig. 7 Equivalence between the $Cp^{\#}_2La$ fragment and two rugby balls

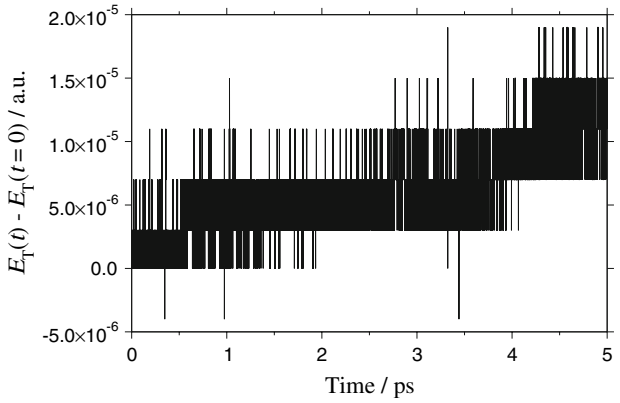

Fig. 8 Evolution of the relative total energy for a trajectory as a function of time. The constraint is fixed to $\xi = 0.5$, which corresponds to the exploration of the transition state region

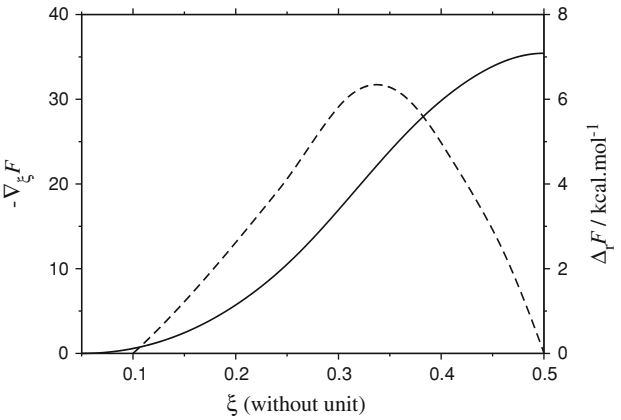

Fig. 9 Evolution of the opposite of the force $-\nabla_\xi \mathcal{F}$ (*dotted line*) of the constraint and the free energy difference $\Delta_r \mathcal{F}$ (*solid line*) obtained after integration

trajectories where the constraint ξ has been fixed to different values in a range of 0.05−0.5. Two properties are plotted on Fig. 9 as a function of the constraint ξ: (a) the opposite of the force of the constraint (Eq. 7) and (b) the free energy difference computed after integration of the force (Eq. 6).

The calculated free energy barrier is found to be 7.1 kcal mol^{-1}, whereas the corresponding barrier computed considering the Cl_2LaH catalyst with the same AIMD methodology [54] is 6.2 kcal mol^{-1}. These close values are in agreement with the fact that the *potential energy* activation barriers $\Delta_r E^{\#}$ are also close (1.43 and 1.93 kcal mol^{-1} with $Cp^{\#}_2LaH$ and Cl_2LaH, respectively). These kinetic data lead us to affirm that anharmonicity effects are of great importance for this reaction. As a matter of fact, they are far away from the corresponding free energy activation barrier computed in the case of the chloride ligand and with the harmonic approximation, $\Delta_r \mathcal{F}^{\#} = 11.2$ kcal mol^{-1}. This discrepancy has already been attributed to anharmonicity

Table 2 Selected distances (in Å) for the hydrogen exchange transition state $Cp_2^{\#}La(H_3)$, see Fig. 6 for atom definition

	Static[a]	Dynamic[b]
$r(La-H^a)$	2.284	2.350 ± 0.069
$r(La-H^b)$	2.257	2.313 ± 0.054
$r(H^a-H^b)$	1.015	1.048 ± 0.027

[a] Bond length from a "static" TS geometry optimization

[b] average values and standard deviations from the $\xi = 0.5$ MD trajectory

effects and the failure of the harmonic approximation usually employed to compute vibrational entropic contributions for free energy. This is due to the flatness of the potential energy surface, a significant number of normal modes of low frequencies (below 500 cm^{-1}) being calculated for the transition state [54].

These anharmonicity effects lead to deviations for some geometrical parameters. Table 2 gathers some selected distances for the transition state. Significant differences occur between the optimized geometry on the potential energy surface and the corresponding values averaged on the $\xi = 0.5$ MD trajectory. These discrepancies strengthen our doubts concerning the relevance of the harmonic approximation for the free energy activation barrier estimation for this hydrogen exchange reaction.

4 Conclusion

Multicentered EGPs have proven their ability to generate a relevant ligand-field in organometallic clusters. It has more specifically been demonstrated in the case of η^6-benzene, which has been added to the EGP library. The remarkably accurate description of the electronic structure, geometry and energy of $[Ru_4(H)_4(C_6H_6)_4]^{n+}$ is very promising. It opens the road to the use of such molecular pseudopotentials in the context of organometallic NPs, where new methodological developments are required in order to reduce the computational cost of DFT calculations. Considering that dynamical effects occur at the surface of organometallic NPs, we have also checked the behavior of EGPs in the context of ab initio molecular dynamics. A prototype system has been considered, namely an hydrogen exchange reaction catalyzed by a Cp_2LaH complex. Energy conservation during 5 ps of this joint EGP/MD is not violated, thus confirming that EGPs do not introduce spurious trajectories in MD simulations. In addition, the barrier height of this reaction, evaluated within the so-called blue-moon algorithm, is in close agreement with reference data. In other words, the part of the potential energy surface associated to the reaction is accurately obtained with EGPs, even the anharmonic part. These results confirm that EGPs could be useful tools in the context of large organometallic clusters. An extension of the EGP library would however require to perform secure extractions of the molecular pseudopotential. Some guidelines are also provided in order to build a new generation of EGPs in a more routine way.

Acknowledgments We thank the CALcul en MIdi-Pyrénées (CALMIP) for generous allocations of computer time. Laurent Maron is member of the Institut Universitaire de France (IUF). Financial support by the CNRS and the ANR (SIDERUS project, ANR-08-BLAN-0010-01 and ANR-08-BLAN-0010-02) is gratefully acknowledged. This work is dedicated to the memory of Dr Jean-Pierre Daudey, who was affectionately called by us "Ze Guru". EGP extractions and applications for benzene, as well as the corresponding sections of this article were essentially achieved during a wonderful week in the département of Ardèche, in April 2009. *Je me souviens* [76, 77] *d'une fameuse fondue au LPQ autour de la table à saucissons. Je me souviens des rires et des doutes existentiels et scientifiques. Je me souviens du xylophone à roulettes d'Emilie que tu faisais tintinabuler pour nous convier à prendre le thé. Je me souviens de la trousse Babar qui t'accompagnait à chaque réunion. Je me souviens des impulsions scientifiques décisives que tu as données à ces travaux, après tant d'autres. Je me souviens de ta mélancolie.*

References

1. Schmid G (ed) (2004) Nanoparticles. From theory to application. Wiley, Weinheim
2. Calvo F, Carré A (2006) Nanotechnology 17:1292–1299
3. del Rosal I, Jolibois F, Maron L, Philippot K, Chaudret B, Poteau R (2009) Dalton Trans 2142–2156
4. Pery T, Pelzer K, Buntkowsky G, Philippot K, Limbach HH, Chaudret B (2005) Chem Phys Chem 6:605–607
5. Schröder F, Esken D, Cokoja M, vanden Berg MWE, Lebedev OI, van Tendeloo G, Walaszek B, Buntkowsky G, Limbach H-H, Chaudret B, Fischer RA (2008) J Am Chem Soc 130:6119–6130
6. Walaszek B, Adamczyk A, Pery T, Yeping X, Gutmann T, de S. Amadeu N, Ulrich S, Breitzke H, Vieth HM, Sabo-Etienne S, Chaudret B, Limbach H-H, Buntkowsky G (2008) J Am Chem Soc 130:17502–17508
7. del Rosal I, Maron L, Poteau R, Jolibois F (2008) Dalton Trans 3959–3970
8. del Rosal I, Gutman T, Maron L, Jolibois F, Philippot K, Chaudret B, Wakaszek B, Limbach HH, Poteau R, Buntkowsky G (2009) Phys Chem Chem Phys 11:5657–5663
9. Buntkowsky G, Limbach HH (2006) J Low Temp Phys 143:55–114
10. Poteau R, Maynau D, Spiegelmann F (1993) Chem Phys 175:289–297
11. Raynaud C, Maron L, Daudey J-P, Jolibois F (2006) ChemPhysChem 7:407–413
12. Raynaud C, Poteau R, Maron L, Jolibois F (2006) J Mol Struct Theochem 771:43–50
13. Raynaud C, Maron L, Daudey J-P, Jolibois F (2004) Phys Chem Chem Phys 6:4226–4232
14. Raynaud C, Daudey J-P, Jolibois F, Maron L (2006) J Phys Chem A 110:101–105
15. Durand P, Malrieu J-P (1987) Advances in chemical physics: ab initio methods in quantum chemistry, vol LXVII, part I. Wiley, New York, pp 321–412
16. Poteau R, Ortega I, Alary F, Ramirez Solis A, Barthelat J-C, Daudey J-P (2001) J Phys Chem A 105:198–205

17. Poteau R, Alary F, el Makarim HA, Heully J-L, Barthelat J-C, Daudey J-P (2001) J Phys Chem A 105:206–214
18. Heully J-L, Poteau R, Berasaluce S, Alary F (2002) J Chem Phys 116:4829–4836
19. Alary F, Heully J-L, Poteau R, Maron L, Trinquier G, Daudey J-P (2003) J Am Chem Soc 125:11051–11061
20. Bessac F, Alary F, Poteau R, Heully J-L, Daudey J-P (2003) J Phys Chem A 107:9393–9402
21. Bessac F, Carissan Y, Alary F, Heully J-L, Daudey J-P, Poteau R (2003) J Mol Struct Theochem 632:43–59
22. Carissan Y, Bessac F, Alary F, Heully J-L, Poteau R (2006) Int J Quant Chem 106:727–733
23. Slavíček P, Martínez TJ (2006) J Chem Phys 124:084107–084110
24. Lewin JL, Cramer CJ (2008) J Phys Chem A 112:12754–12760
25. Albright TA, Burdett JK, Whangbo M-H (1985) Orbital interactions in chemistry. Wiley, New York
26. Durand P, Barthelat J-C (1975) Theor Chim Acta 38:283–302
27. Stevens WJ, Basch H, Krauss M (1984) J Chem Phys 81:6026–6033
28. Hoffmann R (1982) Angew Chem Int ed Eng 21:711–800
29. Pelissier M, Komiha N, Daudey J-P (1988) J Comp Chem 9:298–302
30. Nicolas G, Durand Ph (1980) J Chem Phys 72:453–463
31. Frisch MJ, Trucks GW, Schlegel HB, Scuseria GE, Robb MA, Cheeseman JR, Montgomery JA Jr, Vreven T, Kudin KN, Burant JC, Millam JM, Iyengar SS, Tomasi J, Barone V, Mennucci B, Cossi M, Scalmani G, Rega N, Petersson GA, Nakatsuji H, Hada M, Ehara M, Toyota K, Fukuda R, Hasegawa J, Ishida M, Nakajima T, Honda Y, Kitao O, Nakai H, Klene M, Li X, Knox JE, Hratchian HP, Cross JB, Adamo C, Jaramillo J, Gomperts R, Stratmann RE, Yazyev O, Austin AJ, Cammi R, Pomelli C, Ochterski JW, Ayala PY, Morokuma K, Voth GA, Salvador P, Dannenberg JJ, Zakrzewski VG, Dapprich S, Daniels AD, Strain MC, Farkas O, Malick DK, Rabuck AD, Raghavachari K, Foresman JB, Ortiz JV, Cui Q, Baboul AG, Clifford S, Cioslowski J, Stefanov BB, Liu G, Liashenko A, Piskorz P, Komaromi I, Martin RL, Fox DJ, Keith T, Al-Laham MA, Peng CY, Nanayakkara A, Challacombe M, Gill PMW, Johnson B, Chen W, Wong MW, Gonzalez C, Pople JA (2003) Gaussian 03 (Revision B.05)
32. Dolg M, Wedig U, Stoll H, Preuss H (1987) J Chem Phys 86:866–872
33. Zhang Y, Lee T-S, Yang W (1999) J Chem Phys 110:46–54
34. Dilabio GA, Hurley MM, Christiansen PA (2002) J Chem Phys 116:9578–9584
35. Meister G, Rheinwald G, Stoeckli-Evans H, Süss-Fink G (1994) J Chem Soc Dalton Trans 3215–3223
36. Mingos DMP, Wales DJ (1990) Introduction to cluster chemistry. Prentice-Hall, Englewood Cliffs
37. Fox MA, Wade K (2003) Pure Appl Chem 75:1315–1323
38. Gautier R, Chérioux F, Süss-Fink G, Saillard J-Y (2003) Inorg Chem 42:8278–8282
39. McQuarrie DA (2000) Statistical mechanics, 2nd edn. University Science Books, Sausalito
40. Barone V (2004) J Chem Phys 120:3059–3065
41. Hoover WG (1985) Phys Rev A 31:1695–1697
42. Sprik M, Ciccotti G (1998) J Chem Phys 109:7737–7744
43. Car R, Parrinello M (1985) Phys Rev Lett 55:2471–2474
44. Bolton K, Hase WL, Peslherbe GH (1998) Direct Dynamics of reactive systems. In: Modern methods for multidimensional dynamics computation in chemistry. World Scientific, Singapore, pp 143–189
45. Millam JM, Bakken V, Chen W, Hase WL, Schlegel HB (1999) J Chem Phys 111:3800–3805
46. Li X, Millam JM, Schlegel HB (2000) J Chem Phys 113:10062–10067
47. Marx D, Hutter J (2000) Ab initio molecular dynamics: theory and implementation. In: Modern methods and algorithms of quantum chemistry. John von Neumann Institute for Computing, Forschungszentrum Jülich, Jülich, pp 329–477
48. Hartke B, Carter EA (1992) Chem Phys Lett 189:358–362
49. Radeke MR, Carter EA (1997) Annu Rev Phys Chem 48:243–270
50. Nosé S (1984) J Chem Phys 81:511–519
51. Raynaud C, Maron L, Jolibois F, Daudey J-P, Esteves PM, Ramírez-Solís A (2005) Chem Phys Lett 414:161–165
52. Jolibois F, Maron L, Ramírez-Solís A (2007) Chem Phys Lett 435:34–38
53. Jolibois F, Maron L, Ramírez-Solís A (2009) J Mol Struct Theochem 899:9–17
54. Raynaud C, Daudey J-P, Maron L, Jolibois F (2005) J Phys Chem A 109:9646–9652
55. Watson PL, Parshall GW (1985) Acc Chem Res 18:51–56
56. Ziegler T, Folga E, Berces A (1993) J Am Chem Soc 115:636–646
57. Maron L, Perrin L, Eisenstein O (2002) J Chem Soc Dalton Trans 534–539
58. Perrin L, Maron L, Eisenstein O (2002) Inorg Chem 41:4355–4362
59. Maron L, Werkema EL, Perrin L, Eisenstein O, Andersen RA (2005) J Am Chem Soc 127:279–292
60. Werkema EL, Messines E, Perrin L, Maron L, Eisenstein O, Andersen RA (2005) J Am Chem Soc 127:7781–7795
61. Maron L, Eisenstein O, Alary F, Poteau R (2002) J Phys Chem A 106:1797–1801
62. Frenkel D, Smit B (1996) Understanding molecular simulation—from algorithms to applications. Academic Press, San Diego
63. Torrie GM, Valleau J-P (1974) Chem Phys Lett 28:578–581
64. Torrie GM, Valleau J-P (1977) J Comp Phys 23:187–199
65. Laio A, Parrinello M (2002) Proc Natl Acad Sci USA 99:12562–12566
66. Iannuzzi M, Laio A, Parrinello M (2003) Phys Rev Lett 90:238302
67. Carter EA, Ciccotti G, Hynes JT, Kapral R (1989) Chem Phys Lett 156:472–477
68. Paci E, Ciccotti G, Ferrario G, Kapral R (1991) Chem Phys Lett 176:581–587
69. den Otter WK, Briels WJ (1998) J Chem Phys 109:4139–4146
70. Becke AD (1993) J Chem Phys 98:5648–5652
71. Burke K, Perdew JP, Wang Y (1998) Electronic density functional theory: recent progress and new directions. Plenum, New York
72. Dolg M, Stoll H, Savin A, Preuss H (1989) Theor Chim Acta 75:173–194
73. Hariharan PC, Pople JA (1973) Theor Chem Acc 28:213–222
74. Frisch MJ, Trucks GW, Schlegel HB, Scuseria GE, Robb MA, Cheeseman JR, Zakrzewski VG, Montgomery JA Jr, Stratmann RE, Burant JC, Dapprich S, Millam JM, Daniels AD, Kudin KN, Strain MC, Farkas O, Tomasi J, Barone V, Cossi M, Cammi R, Mennucci B, Pomelli C, Adamo C, Clifford S, Ochterski J, Petersson GA, Ayala PY, Cui Q, Morokuma K, Malick DK, Rabuck AD, Raghavachari K, Foresman JB, Cioslowski J, Ortiz JV, Baboul AG, Stefanov BB, Liu G, Liashenko A, Piskorz P, Komaromi I, Gomperts R, Martin RL, Fox DJ, Keith T, Al-Laham MA, Peng CY, Nanayakkara A, Gonzalez C, Challacombe M, Gill PMW, Johnson BG, Chen W, Wong MW, Andres JL, Head-Gordon M, Replogle ES, Pople JA (1998) Gaussian 98 (Revision A.11)
75. Verlet L (1967) Phys Rev 159:98–103
76. Perec G (1978) Je me souviens, Les Choses Communes I. Hachette (collection P.O.L.), Paris, France
77. Brasseur R (2003) Je me souviens encore mieux de Je me souviens: Notes pour Je me souviens de Georges Perec á l'usage des générations oublieuses et de celles qui n'ont jamais su. Castrol Astral, Pantin, France